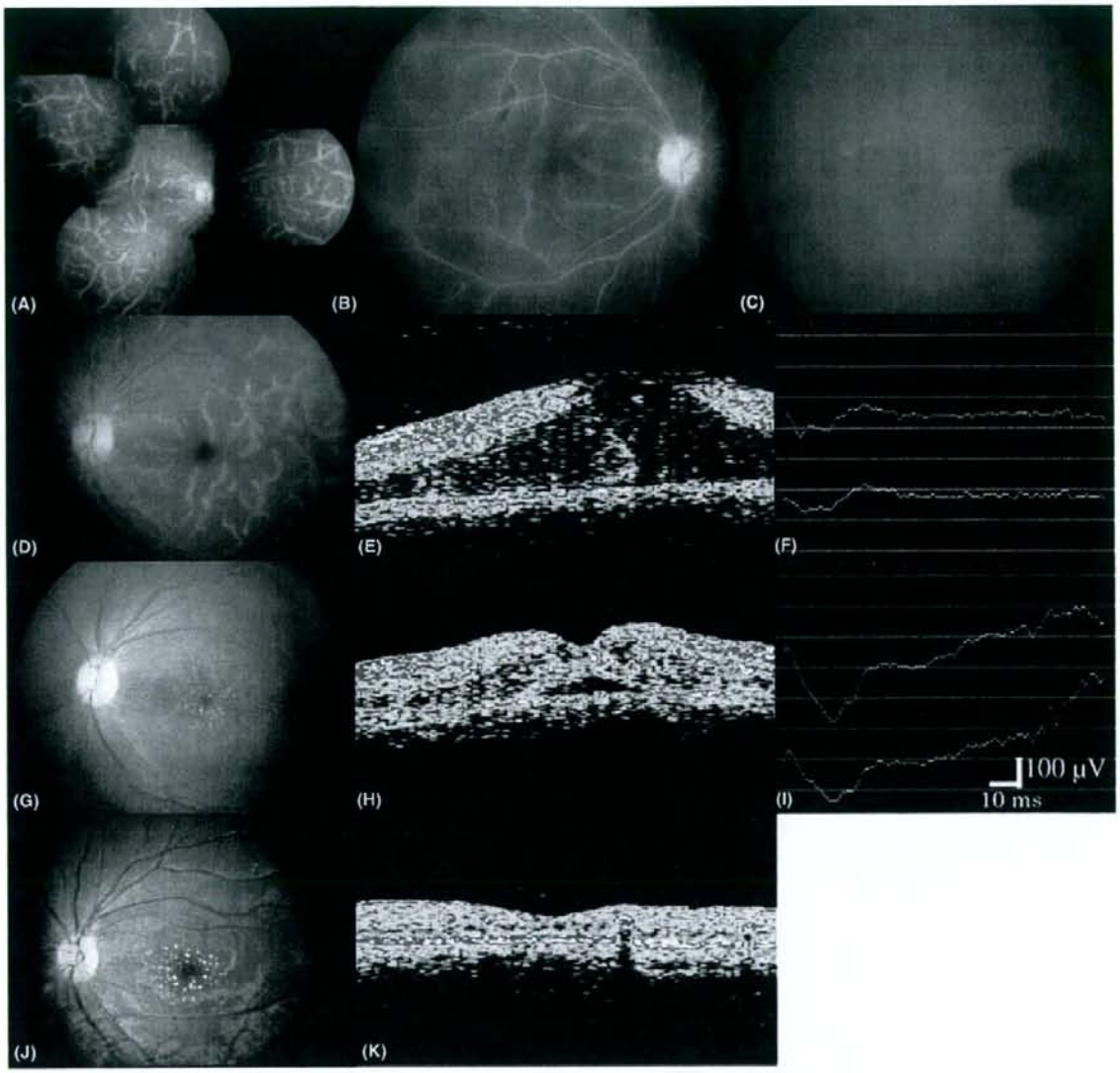

Fig. 1. Fundus photographs, angiograms, optical coherence tomography (OCT) images and electroretinograms (ERGs) in a patient with frosted branch angiitis. (A) Initial fundus appearance of the right eye shows diffuse perivascular white sheathing affecting both veins and arteries. Visual acuity was 0.15 OD. (B) Fluorescein angiography before treatment shows extensive dye leakage from both veins and arteries. Optic discs are hyperfluorescent at the late phase. (C) Indocyanine green angiography before treatment shows mottled pattern of background dye and vessel staining, and hypofluorescence at the disc with blurred margin. (D, E) Initial fundus photograph and OCT image show frosted branch angiitis and prominent macular oedema in the left eye. Visual acuity was 0.1 OS. (F) ERG recorded at the initial visit shows reduced amplitudes of the a- and b-waves and the oscillatory potentials. (G, H) Seven days after the initial visit (see D and E), angiitis is absent and satellite-shaped exudates are present. OCT shows a reduction of oedema but the foveal detachment is still present. Visual acuity was 0.3 OD and 0.3 OS. (I) ERG recorded 7 days after the initial visit (see F) shows marked recovery, but the a- and b-waves and the oscillatory potentials are still not completely recovered. (J, K) At 60 days after the initial visit, macular exudates are still present but OCT shows complete resolution of the macular oedema and foveal detachment. Visual acuity was 0.8 OD and 1.0 OS.

The changes in the macular pathology of our subject during the recovery phase provided two insights. Firstly, despite the essential resolution of the macular oedema, the relatively long period of serous detachment points to the longterm effects of retinal angiitis in altering the outer retinal layer, retinal pigment epithelium and choroid. The reduced ERGs and abnormal angiographic findings support this prolonged effect. These abnormalities accounted for the visual dysfunction.

Secondly, visual improvement in our subject depended on the complete recovery of the macula pathology following the resolution of the retinal angiitis. Non-invasive monitoring of macular changes was valuable in evaluating the course of the disease and

the effects of treatment. The efficacy of steroid is still debatable, but, although our findings pertain to only one case of FBA, we believe that the prompt institution of steroids led to the rapid resolution of peripheral angiitis and macular alterations.

The exact pathogenesis of FBA has not been determined, but it has been linked to a variety of infective agents. Thus, FBA has been suggested to represent the response to a common immunological pathway (Kleiner 1997; Walker et al. 2004). Kleiner (1997) stated that FBA develops in association with a lymphoma (first group), a viral or infectious agent (second group), or idiopathically (third group). In our case, a flu-like episode with fever preceded the ocular symptoms. The high titres of ASO and ASK were suggestive of a streptococcal infection. This supports an earlier report of a positive serology for ASO in patients with FBA (Kleiner et al. 1988). In addition, immunological mimicry between retinal S-antigen and group A streptococcal M proteins has been suggested (Lerner et al. 1995). Thus, routine serological checks for ASO or ASK should be helpful in determining whether FBA is associated with a streptococcal infection or has an underlying immune cross-reactivity.

Acknowledgements

Support for this study was provided by Researches on Sensory and Communicative Disorders from the Ministry of Health, Labour and Welfare, Japan.

References

Kleiner RC (1997): Frosted branch angiitis: clinical syndrome or clinical sign? Retina **17**: 370–371.

Kleiner RC, Kaplan HJ, Shakin JL, Yannuzzi LA, Crosswell HH Jr & McLean WC Jr (1988): Acute frosted retinal periphlebitis. Am J Ophthalmol **106**: 27–34.

Lerner MP, Donoso LA, Nordquist RE & Cunningham MW (1995): Immunological mimicry between retinal S-antigen and group A streptococcal M proteins. Autoimmunity **22**: 95–106.

Walker S, Iguchi A & Jones NP (2004): Frosted branch angiitis: a review. Eye **18**: 527–533.

Received on March 27th, 2008.
Accepted on April 20th, 2008.

Correspondence:
Kei Shinoda MD, PhD
Department of Brain and Neuroscience
Division of Sensory and Locomotive Science
Ophthalmology
Oita University Faculty of Medicine
Hasama-machi
Yufu-shi
Oita 879-5593
Japan
Tel: + 81 97 549 4411 (ext. 5901)
Fax: + 81 97 549 6043
Email: shinodak@med.oita-u.ac.jp

Journal of Medical Case Reports

BioMed Central

Case report

Open Access

Vitrectomy combined with glial tissue removal at the optic pit in a patient with optic disc pit maculopathy: a case report

Makoto Inoue*[1,2], Kei Shinoda[1] and Susumu Ishida[1]

Address: [1]Department of Ophthalmology, Keio University School of Medicine, Shinanomachi, Shinjuku-ku, Tokyo 160-8582, Japan and [2]Kyorin Eye Center, Kyorin University School of Medicine, Shinkawa, Mitaka, Tokyo 181-8611, Japan

Email: Makoto Inoue* - inoue@eye-center.org; Kei Shinoda - shinodak@med.oita-u.ac.jp; Susumu Ishida - ishidasu@sc.itc.keio.ac.jp

* Corresponding author

Published: 7 April 2008

Journal of Medical Case Reports 2008, **2**:103 doi:10.1186/1752-1947-2-103

Received: 19 November 2007
Accepted: 7 April 2008

This article is available from: http://www.jmedicalcasereports.com/content/2/1/103

Abstract

Introduction: We present a case of a man with optic disc pit maculopathy, whose vision improved after vitrectomy combined with glial tissue removal from the optic pit area, and without the use of photocoagulation.

Case presentation: A 45-year-old man complained of blurred vision, and ophthalmoscopy revealed a retinal detachment and retinoschisis extending from an optic disc pit through the macula in his left eye. He was diagnosed with optic disc pit maculopathy, and vitrectomy was performed. A posterior vitreous detachment was created, glial tissue at the optic pit was removed, and octafluoropropane (C_3F_8) was injected as a gas tamponade. The retinal detachment and retinoschisis disappeared after six months, and vision improved to 20/20 without any visual field defects (Goldmann perimetry). A cataractous lens was extracted 2 years after the vitrectomy, and vision has remained 20/20 for 10 years without any recurrence.

Conclusion: The removal of glial tissue during vitrectomy may be beneficial in patients with optic disc pit maculopathy.

Introduction

Optic disc pit maculopathy is characterized by a congenital optic disc pit associated with a macular detachment and retinoschisis [1]. Focal laser photocoagulation of the temporal juxtapapillary retina or vitrectomy combined with a gas tamponade has been reported to be effective in treating this syndrome [1,2]. However, a relatively high incidence of recurrence has been reported after laser treatment alone [1]. A combination of both procedures has recently been reported to be an effective treatment [3].

Glial tissue is occasionally seen in the optic disc pit of patients with an optic disc pit or coloboma, but the reason for its development is unknown. We report a case of a man with optic disc pit maculopathy that was successfully treated using vitrectomy combined with the removal of glial tissue from the optic disc pit followed by the use a gas tamponade.

Case presentation

A 45-year-old Japanese man visited our clinic in September 1996 complaining of decreased vision in his left eye. His vision was decreased to 20/200, and ophthalmoscopy showed a retinal detachment involving the macula and a retinoschisis that extended from the optic disc pit through the macula in the left eye (Figure 1A). Glial tissue was seen at the optic disc pit but a retinal tear was not seen. Fluorescein angiography showed hypofluorescence of the

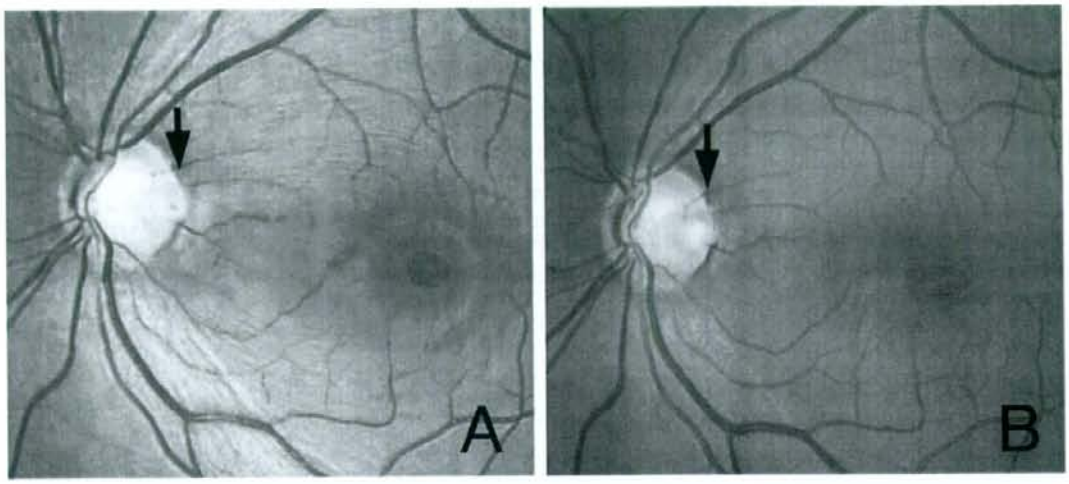

Figure 1
Fundus photograph of the left eye before and after vitreous surgery. (A) Retinal detachment and retinal schisis can be seen with a double ring apparatus. Glial tissue can be seen at the optic pit (arrow). (B) Fundus photograph of the left eye four years after vitreous surgery. Retinal detachment and retinoschisis are absent and the excavation of the optic disc is clearly seen after removal of the glial tissue (arrow).

optic disc pit, and multiple hyperfluorescent spots in the area of the macular lesion (Figure 2), but with no dye leakage. In the late phase, the optic disc pit and glial tissue became hyperfluorescent with mild dye leakage. He was diagnosed with optic disc pit maculopathy and vitrectomy was recommended.

After obtaining informed consent, vitrectomy was performed. A posterior vitreous detachment (PVD) was created by suction with a vitreous cutter until the 'fish-strike sign' was no longer seen. However, the vitreous cortex remained firmly attached at the optic disc pit. Neither condensed vitreous strands nor a residual Cloquet's canal

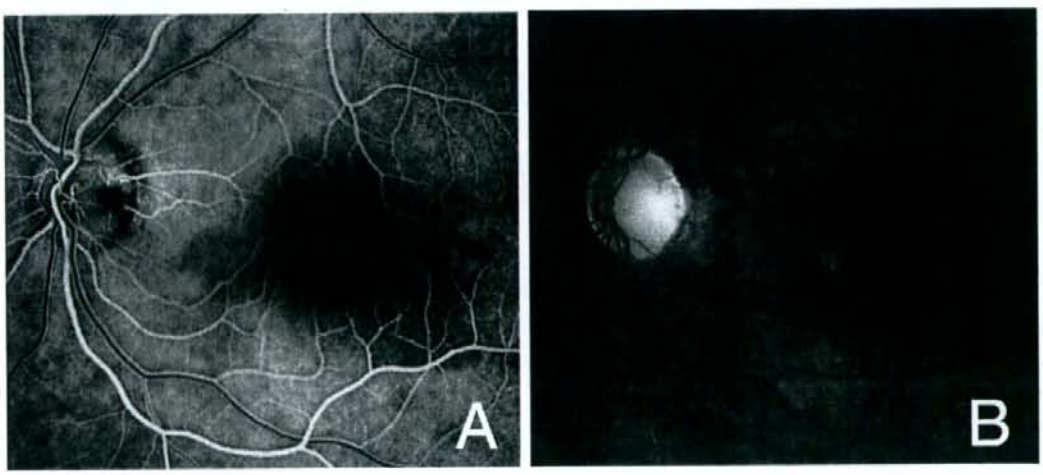

Figure 2
Fluorescein angiograms of the left eye. (A) Fluorescein angiogram in the early phase showing hypofluorescence at the optic pit and many hyperfluorescence spots can be seen in the macular lesion.(B) The hypofluorescence at the optic pit and glial tissue turned to hyperfluorescence with weak dye leakage in the late phase.

was observed. It was decided intra-operatively that the glial tissue at the edge of the optic pit should be removed in order to remove the vitreous traction completely. Tapered forceps with a fine tip were used to avoid contact with the neural tissue at the edges of the optic pit. During this procedure, it was noted that the glial tissue was firmly attached to the temporal wall of the optic pit. An excavated space at the bottom of the optic pit was then clearly observed after removal of the tissue.

The vitrectomy was completed with a 14% octafluoropropane (C_3F_8) gas tamponade, and the patient was instructed to maintain a face-down position for a week. Under these conditions, the retinal detachment and retinoschisis gradually decreased, and the retinal detachment and retinoschisis were absent six months postoperatively (Figure 1B). Vision improved to 20/20 without any visual field defects (Goldmann perimetry).

The patient's vision deteriorated to 20/40 owing to a nuclear sclerosis cataract two years after the vitrectomy, and the lens was extracted. Vision has remained 20/20 for 10 years without any recurrence of the retinal detachment or retinoschisis. Optical coherence tomography (OCT) at this time did not detect a retinal detachment or retinoschisis, but two channels were seen running from the vitreous cavity to the longitudinal space of the optic nerve, possibly the subarachnoid space and the intraretinal space. The exit of these channels to the vitreous cavity was closed (Figure 3).

Discussion

The mechanism causing optic disc pit maculopathy has been considered to be vitreous traction on the optic disc pit. Bonnet [4] reported that 25 eyes with a macular detachment associated with an optic disc pit did not have a PVD, and two of the eyes had a reattachment of the macula after the development of a spontaneous PVD. Akiba et al [5] noted a residual Cloquet's canal moving in concert with a pulsating translucent membrane over the optic disc pit to cause anterior-posterior vitreous traction. However, the source of the subretinal fluid that causes the macular detachment and retinoschisis is still controversial, that is, whether it is vitreous fluid or cerebrospinal fluid [6].

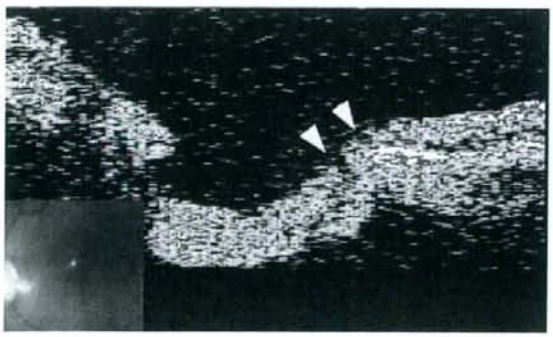

Figure 3
OCT image seven years after vitrectomy. Cross section of the temporal side of the optic disc showing two channels (arrowheads) connecting the vitreous cavity to the longitudinal space of the optic nerve and to the intraretinal space. The exit to the vitreous cavity is closed.

The effectiveness of vitreous surgery to create a PVD around the optic disc with or without laser treatment has been examined [2,3]. The serous macular detachment associated with optic pits probably has a rhegmatogenous component. Thus, Postel et al [6] described a hole or tear in the diaphanous tissue overlying the optic pit in all of their seven cases. Todokoro et al [7], using careful OCT examinations, observed a cystic cavity covered with a superficial layer of optic disc tissue in a patient with a retinal detachment and retinoschisis that might correspond with the translucent membrane over the optic disc pit.

OCT was not performed preoperatively in our case, and the connection between the glial tissue and the optic disc pit was only detected intra-operatively. We suggest that the glial tissue might have developed after continuous vitreous traction of the vitreous strand attached to the optic disc pit. Thus, removal of the glial tissue might have made it possible to remove the vitreous traction completely, or to seal the retinal break at the optic disc pit by removing the translucent membrane and glial tissue associated with the wound healing process to close the two intraretinal channels seen in the OCT images. On the other hand, the procedures might have enlarged the retinal break in the pit or damaged the nerve fibres at the optic disc. A permanent escape may be produced mechanically by displacement of the fluid during vitreous surgery and the use of a gas tamponade, and the retina flattens with time even though the flow from the subarachnoid space remains constant. A reservoir for the fluid from the subarachnoid space might be the vitreous cavity with an egress into it provided by some retinal fenestration near the optic nerve head [8].

We cannot make a strong conclusion on the efficacy of the removal of the glial tissue based on a single case. However, considering the absence of any side-effects, such as visual field defects or decreased vision, removal of glial tissue may be beneficial in selected cases. Additional studies with larger samples are needed to evaluate the efficacy of glial removal.

Conclusion
The removal of glial tissue during vitrectomy may be beneficial in patients with optic disc pit maculopathy.

Competing interests
The author(s) declare that they have no competing interests.

Authors' contributions
MI evaluated the patients and performed vitreous surgery. KS and SI reviewed the manuscript.

Consent
Written informed consent was obtained from the patient for publication of this case report and accompanying images. A copy of the written consent is available for review by the Editor-in-Chief of this journal.

References
1. Gass JD: **Serous detachment of the macula. Secondary to congenital pit of the optic nerve head.** *Am J Ophthalmol* 1969, **67**:821-841.
2. Hirakata A, Okada AA, Hida T: **Long-term results of vitrectomy without laser treatment for macular detachment associated with an optic disc pit.** *Ophthalmology* 2005, **112**:1430-1435.
3. Garcia-Arumi J, Guraya BC, Espax AB, Castillo VM, Ramsay LS, Motta RM: **Optical coherence tomography in optic pit maculopathy managed with vitrectomy-laser-gas.** *Graefes Arch Clin Exp Ophthalmol* 2004, **242**:819-826.
4. Bonnet M: **Serous macular detachment associated with optic nerve pits.** *Graefes Arch Clin Exp Ophthalmol* 1991, **229**:526-532.
5. Akiba J, Kakehashi A, Hikichi T, Trempe CL: **Vitreous findings in cases of optic nerve pits and serous macular detachment.** *Am J Ophthalmol* 1993, **116**:38-41.
6. Postel EA, Pulido JS, McNamara JA, Johnson MW: **The etiology and treatment of macular detachment associated with optic nerve pits and related anomalies.** *Trans Am Ophthalmol Soc* 1998, **96**:73-88.
7. Todokoro D, Kishi S: **Reattachment of retina and retinoschisis in pit-macular syndrome by surgically-induced vitreous detachment and gas tamponade.** *Ophthalmic Surg Lasers* 2000, **31**:233-235.
8. Hotta K: **Unsuccessful vitrectomy without gas tamponade for macular retinal detachment and retinoschisis without optic disc pit.** *Ophthalmic Surg Lasers Imaging* 2004, **35**:328-331.

LETTERS

Visual perception of luxated intraocular lens by the patient

We examined a patient with a luxation of an encapsulated intraocular lens (IOL) who clearly perceived and drew detailed images of the IOL.

CASE REPORT

A 74-year-old woman underwent vitrectomy with phacoemulsification, and a three-piece soft acrylic IOL (+23.5 D, MA60BM; Alcon, Fort Worth, TX) was implanted into the posterior chamber of the right eye uneventfully for vitreous opacity associated with sarcoidosis in 2002. Five years later, she noticed a sudden decrease in vision in the right eye. Ophthalmoscopy revealed a luxation of the encapsulated IOL onto the retina (fig 1). She made a drawing showing what she saw with her right eye (fig 1). Fundus examination confirmed that the direction of the IOL had not changed before and after she made the drawing. The shape and colour of the IOL had not been shown or described to the patient previously, and the drawings were based only on her perception.

The luxated IOL was removed, and another IOL was sutured to the ciliary sulcus. Her corrected visual acuity was 20/20 after the surgery.

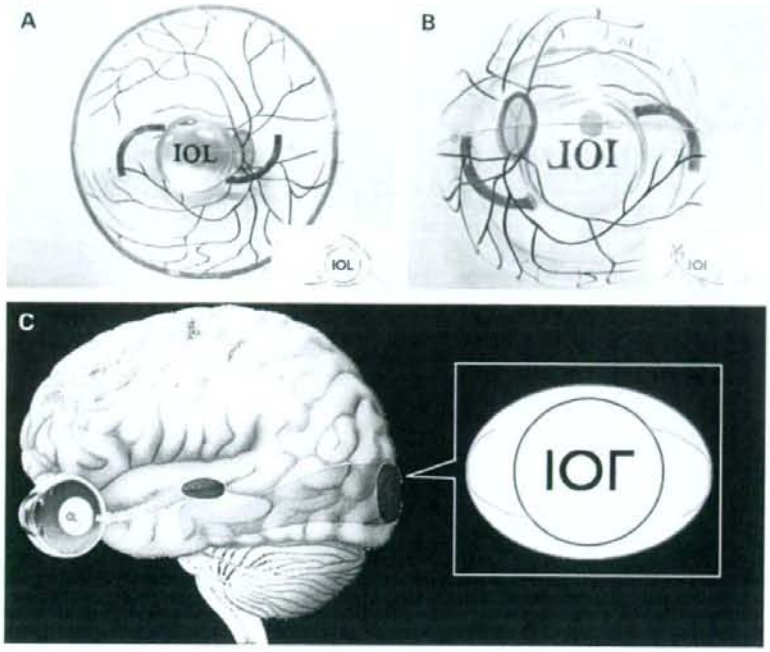

Figure 2 Relationship between the fundus photograph and the patient's drawing. (A) Intraocular lens (IOL) on the macula in an eye cup model simulating an IOL in the patient's fundus (fig 1A). Inset : diagram of the IOL. (B) Appearance from the back of the eye. Note that the characters "IOL" are flipped horizontally. Inset: diagram of the IOL. (C) Diagram showing how the patient perceived the IOL on her retina. The patient's perception should be vertically and horizontally reversed from the (B) inset. Note that (C) is exactly the same but only the vertical reversal of the inset in (A). Therefore, it is reasonable that fig 1C resembles precisely fig 1B.

COMMENTS

The visual sensations perceived by patients during vitreous surgery have been well documented such as lights,[1–3] one or more colours,[2 4 5] instruments,[3–5] etc. Sugisaka *et al*[6] suggested that the patient saw the shadow of the instruments, but this cannot completely explain the patient's perception during vitrectomy because some of the patients reported perceiving haemorrhages as red and vitreous forceps as gold.

As shown in fig 2, it was reasonable that the patient's drawing (fig 1C) resembled precisely only the vertically reversed fundus picture (fig 1B). Our patient's descriptions had characteristics that were similar to those reported during vitrectomy, suggesting that the same undetermined mechanism

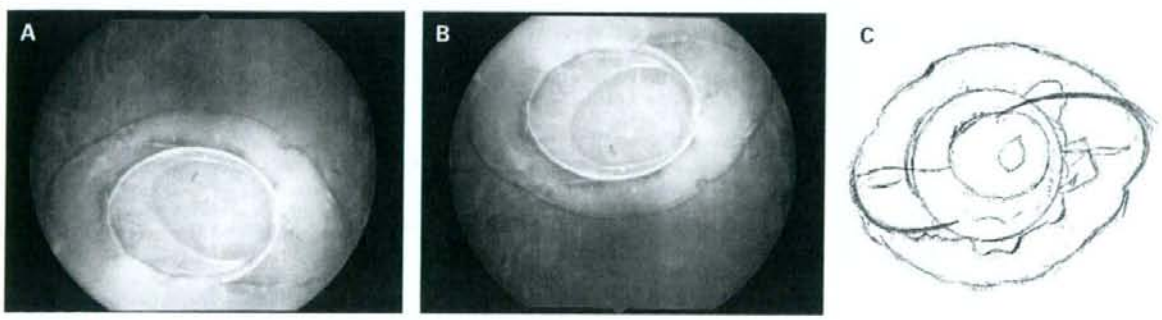

Figure 1 Fundus photograph showing the luxated encapsulated intraocular lens (IOL) on the retina and drawings by the patient. (A) Fundus photograph taken by a fundus camera when the patient looked down with her face straight ahead. The capsular bag is ellipsoidal, and the loops of the IOL form the major axis of the ellipse. The edge of the capsulorhexis retained its original shape, and the Soemmerring ring was present surrounding the optics of the IOL. (B) Part (A) has been flipped vertically. (C) Drawings by the patient. The object rotated and the position of the green/blue lines changed depending on her head position. Note that part (C) is similar to part (B). The probable mechanism is shown in fig 2.

may underlie the visual perception of the IOL. Additional investigations are needed to determine the mechanism for these phenomena.

T Ikebe,[1] Y Takaki,[2] D Kishi,[2] H Kono,[2] K Shinoda,[2] M Inoue,[3] K Nakatsuka[2]

[1]Department of Ophthalmology, Oita Prefectural Hospital, Oita, Japan; [2]Department of Brain and Neuroscience, Division of Sensory and Locomotive Science, Ophthalmology, Oita University Faculty of Medicine, Oita, Japan; [3]Department of Ophthalmology, Kyorin University School of Medicine, Tokyo, Japan

Correspondence to: Dr K Shinoda, Department of Brain and Neuroscience, Division of Sensory and Locomotive Science, Ophthalmology, Oita University Faculty of Medicine, Hasama-machi, Yufu-shi, Oita 879-5593, Japan; shinodak@med.oita-u.ac.jp

Funding: Support for this study was provided by Research Grants on Sensory and Communicative Disorders from the Ministry of Health, Labor, and Welfare, Japan.

Competing interests: None.

Patient consent: Obtained.

Accepted 17 February 2008

Br J Ophthalmol 2008;**92**:1563–1564. doi:10.1136/bjo.2008.138339

REFERENCES

1. **Mandelcorn MS,** Mandelcorn E, Ananthanarayan C, *et al*. Some observations concerning visual perception during vitrectomy after retrobulbar anesthesia. *Can J Ophthalmol* 1997;**32**:255–6.
2. **Tan CS,** Mahmood U, O'Brien PD, *et al*. Visual experiences during vitreous surgery under regional anesthesia: a multicenter study. *Am J Ophthalmol* 2005;**140**:971–5.
3. **Kawaguchi N,** Inoue M, Sugisaka E, *et al*. Subjective visual sensation during vitrectomy under retrobulbar anesthesia. *Am J Ophthalmol* 2006;**141**:407–9.
4. **Sugisaka E,** Shinoda K, Ishida S, *et al*. Visual sensations during vitrectomy. *Ophthalmology* 2006;**113**:1886.
5. **Sugisaka E,** Shinoda K, Ishida S, *et al*. Patients' descriptions of visual sensations during pars plana vitrectomy under retrobulbar anesthesia. *Am J Ophthalmol* 2007;**144**:245–51.

Age-related macular degeneration and mortality from cardiovascular disease or stroke

We read with interest the article from the Blue Mountains Eye Study reporting a prospective association of age-related macular degeneration (AMD) to cardiovascular disease mortality in an Australian population.[1] This study provides further evidence that both AMD and thromboembolic vascular diseases may share similar risk factors and underlying pathogenetic mechanisms, and is in keeping with the findings from other studies.[2]

It is peculiar that the major significant findings in this study relate only to those patients aged <75 years. As the authors acknowledge, the reasons for this are unclear and need to be explored further. We should point out that the association of mortality with cardiovascular risk, such as blood pressure and cholesterol, are also attenuated in older compared with younger people in many epidemiological studies.[3 4] We also suggest that examining the causes of death in older and younger persons may provide insights to explain this age interaction.

The other major finding of this study was that late AMD was associated with a fivefold higher cardiovascular mortality and a 10-fold higher stroke mortality, again only among persons aged <75 years. This association, however, should be interpreted cautiously, as common risk factors, such as smoking[5] and obesity,[6] are associated with late AMD and are established risk factors for cardiovascular and cerebrovascular disease. Unfortunately, the authors could not adjust for these and other important confounders that could have explained this association, due in part to the small number of people with late AMD in the study. Larger studies, longer follow-up and pooling of existing population cohort studies to provide a greater number of late AMD cases will help elucidate the independent association of late AMD and cardiovascular mortality.

Finally, these data may have implications for current treatments of AMD. The use of antivascular endothelial growth factor (VEGF) therapy in the management of AMD is now widespread, and is backed by robust efficacy data. However, long-term safety data concerning these treatments remain unclear. A possible increased risk of both cardiovascular and cerebrovascular complications associated with anti-VEGF treatment has been suggested.[7] Most recently, the SAILOR (Safety Assessment of Intravitreal Lucentis for Age-related Macular Degeneration) study showed that for patients with a prior history of stroke, a trend towards a higher incidence of stroke was seen in the 0.5 mg ranibizumab dose group compared with the 0.3 mg group.[8] With increasing evidence to suggest that AMD and thromboembolic diseases are linked, we agree with the authors that caution is needed with the use of anti-VEGF therapies in wet AMD patients, particularly those with pre-existing cardiovascular or cerebrovascular disease.

P Cackett,[1,2] N Cheung,[3] T Y Wong[1,2,3,4]

[1]Singapore Eye Research Institute, Singapore; [2]Singapore National Eye Center, Singapore; [3]Centre for Eye Research Australia, University of Melbourne, Australia; [4]Department of Ophthalmology, Yong Loo Lin School of Medicine, National University of Singapore, Singapore

Correspondence to: Professor T Y Wong, Centre for Eye Research Australia, the University of Melbourne, 32 Gisborne Street, Melbourne 3002, Victoria, Australia; twong@unimelb.edu.au

Competing interests: None.

Accepted 4 May 2008

Br J Ophthalmol 2008;**92**:1564. doi:10.1136/bjo.2008.143875

REFERENCES

1. **Tan JS,** Wang JJ, Liew G, *et al*. Age-related macular degeneration and mortality from cardiovascular disease or stroke. *Br J Ophthalmol* 2008;**92**:509–12.
2. **Tan JS,** Mitchell P, Smith W, *et al*. Cardiovascular risk factors and the long-term incidence of age-related macular degeneration: the Blue Mountains Eye Study. *Ophthalmology* 2007;**114**:1143–50.
3. **Langer RD,** Ganiats TG, Barrett-Connor E. Paradoxical survival of elderly men with high blood pressure. *BMJ* 1989;**298**:1356–7.
4. **Howard G,** Manolio TA, Burke GL, *et al*. Does the association of risk factors and atherosclerosis change with age? An analysis of the combined ARIC and CHS cohorts. The Atherosclerosis Risk in Communities (ARIC) and Cardiovascular Health Study (CHS) investigators. *Stroke* 1997;**28**:1693–701.
5. **Tomany SC,** Wang JJ, Van Leeuwen R, *et al*. Risk factors for incident age-related macular degeneration: pooled findings from 3 continents. *Ophthalmology* 2004;**111**:1280–7.
6. **Seddon JM,** Cote J, Davis N, *et al*. Progression of age-related macular degeneration: association with body mass index, waist circumference, and waist-hip ratio. *Arch Ophthalmol* 2003;**121**:785–92.
7. **Wong TY,** Liew G, Mitchell P. Clinical update: new treatments for age-related macular degeneration. *Lancet* 2007;**370**:204–6.
8. **Boyer D.** SAILOR 12-month efficacy and safety results (Cohort 1). In: *Angiogenesis, Exudation, and Degeneration Meeting*, 23 February 2008, Miami, FL. Bascom Palmer Eye Institute.

Method to increase the sensitivity of perimetric trend progression analysis

Gardiner and Crabb reported in the *British Journal of Ophthalmology*[1] that, when applying point by point regression models to evaluate perimetric progression, little information is gained by performing more than three perimetric tests a year because of threshold fluctuation. Increasing this frequency improves sensitivity but worsens specificity. Their criterion allows detection of progression in the range of 1–2 dB/year.

Threshold fluctuation may be reduced by applying mathematical filtering procedures, averaging the value of each threshold with those surrounding it or with those functionally related to it.[2–4] This procedure conserves most of the topographic information and may reduce fluctuation, although only partially.

To overcome the limitations described by Gardiner and Crabb, we have proposed using the analysis of defect or Bebie curve,[5] in which defects are ordered from least to greatest (fig 1).[6] We have called this method Threshold Noiseless Trend.

We have tested its utility in a simulation model: to a theoretical visual field in which all thresholds had around the same value (30 dB), we applied a decrease of 0.5 dB/year to test sensitivity and zero decrease (0 dB/year) to test specificity. We simulated seven quarterly examinations adding a fluctuation of 2.0 dB to each threshold. Thresholds were

The American Journal of Pathology, Vol. 172, No. 5, May 2008

DOI: 10.2353/ajpath.2008.070730

Metabolic, Endocrine and Genitourinary Pathobiology

Retinal Dysfunction and Progressive Retinal Cell Death in SOD1-Deficient Mice

Kouhei Hashizume,*† Manabu Hirasawa,* Yutaka Imamura,* Setsuko Noda,‡ Takahiko Shimizu,§ Kei Shinoda,¶‖ Toshihide Kurihara,* Kousuke Noda,* Yoko Ozawa,* Susumu Ishida,* Yozo Miyake,¶ Takuji Shirasawa,§ and Kazuo Tsubota*

From the Department of Ophthalmology, Inaida Laboratory, Keio University School of Medicine, Tokyo; the Department of Ophthalmology,† Iwate Medical University School of Medicine, Morioka; the Department of Health Science,‡ Tokai University School of Nursing, Kanagawa; the Research Team for Molecular Biomarkers,§ Tokyo Metropolitan Institute of Gerontology, Tokyo; the Department of Ophthalmology,¶ National Institute of Sensory Organs, Tokyo Medical Center, Tokyo; and the Department of Ophthalmology,‖ Oita University School of Medicine, Oita, Japan

The superoxide dismutase (SOD) family is a major antioxidant system, and deficiency of Cu,Zn-superoxide dismutase (SOD1) in mice leads to many different phenotypes that resemble accelerated aging. The purpose of this study was to examine the morphology and physiology of the sensory retina in *Sod1*$^{-/-}$ mice. The amplitudes of the a- and b-waves of electroretinograms elicited by stimuli of different intensity were reduced in senescent *Sod1*$^{-/-}$ mice, and this reduction in amplitude was more pronounced with increasing age. Retinal morphometric analyses showed a reduced number of nuclei in both the inner nuclear cell layer and outer nuclear cell layer. Electron microscopy revealed swollen cells and degenerated mitochondria in the inner nuclear cell and outer nuclear cell layer of senescent *Sod1*$^{-/-}$ mice indicating necrotic cell death. Terminal deoxynucleotidyl transferase-mediated dUTP nick end labeling revealed no significant differences in the number of apoptotic cells between *Sod1*$^{-/-}$ and wild-type mice, and activated caspase-3 could not be detected in the retina of *Sod1*$^{-/-}$ mice. In addition to the age-related macular degeneration-like phenotypes previously reported, *Sod1*$^{-/-}$ mice also present progressive retinal degeneration. Our results indicate that *Sod1*$^{-/-}$ mice may be a good model system in which to study the mechanism of reactive oxygen species-mediated retinal degeneration. *(Am J Pathol 2008, 172:1325–1331; DOI: 10.2353/ajpath.2008.070730)*

The superoxide dismutase (SOD) family is one of the main antioxidant systems in the body and is made up of the three SOD isoenzymes: Cu,Zn-superoxide dismutase (SOD1) exists in the cytoplasm, SOD2 or Mn-SOD in the mitochondrial matrix, and SOD3 or extracellular SOD in the interstitium of tissues as the secreted form.[1] SOD1 catalyzes superoxide radical dismutation and is distributed throughout the body,[1] and among the three isozymes, it is the most abundant in the retina.[2] This suggests that SOD1 may be important in protecting the sensory retina from the reactive oxygen species (ROS)-mediated retinal damage.

Many models of retinal degeneration have been studied[3,4] however, the mechanism of retinal cell deaths in some of these models has still not been determined. Cell death can be either necrotic or apoptotic, and necrotic cell death is characterized by a swelling of the cell membranes and organelles that leads to a disruption of the cell membranes and lysis. These alterations subsequently lead to inflammatory responses.[5] Apoptosis is a process of programmed cell death, and involves an orchestrated series of biochemical events leading to characteristic cell morphology and death. In some models of retinal degeneration, the death of the neurons has been shown to be attributable to apoptosis.[6–8]

SOD1 deficiency (*Sod1*$^{-/-}$) leads to many different phenotypes resembling aging, and the changes are attributable to an elevation of ROS.[9,10] We recently reported that senescent *Sod1*$^{-/-}$ mice had features of age-related macular degeneration (AMD) including the presence of drusen, choroidal neovascularization, and retinal pigment epithelium dysfunction.[11] Because SOD1 is expressed throughout the retina and not only in the retinal pigment epithelium,[11] we have hypothesized that the SOD1 deficiency will alter the morphology and physiology of the retina of *Sod1*$^{-/-}$ mice. To examine this hypothesis, we investigated the morphology of the retina of *Sod1*$^{-/-}$ mice of different ages by morphometric meth-

Accepted for publication January 24, 2008.

K.H. and M.H. contributed equally to this study.

Present address of T.S.: Department of Aging Control Medicine, Juntendo University Graduate School of Medicine, Tokyo, Japan.

Address reprint requests to Yutaka Imamura, M.D., Department of Ophthalmology, Inaida Laboratory, Keio University School of Medicine, 35 Shinanomachi, Shinjuku-ku, Tokyo 160-8582, Japan. E-mail: imamura@sc.itc.keio.ac.jp.

ods and the retinal function by electroretinography. We shall show that the amplitudes of the electroretinograms (ERGs) elicited by different light stimuli were reduced in senescent *Sod1*$^{-/-}$ mice. Morphometric analyses of the retina of *Sod1*$^{-/-}$ mice of different ages showed evidence of necrotic cell death in the retinal cell layers.

Materials and Methods

Animals

Sod1$^{-/-}$ mice that were backcrossed to C57BL/6 and wild-type (WT) mice were studied.[11] All animal experiments were performed in accordance with the Association for Research in Vision and Ophthalmology Statement for the Use of Animals in Ophthalmic and Vision Research.

ERGs

ERGs were recorded as described in detail.[12–14] Briefly, animals were dark-adapted for at least 12 hours and prepared under dim red illumination. A contact lens electrode carrying light-emitting diodes (WLS-20, Mayo Corporation, Inazawa, Japan) was used for the recordings and stimulations. The ERGS were differentially amplified and filtered with the band pass filters set from 0.3 to 500 Hz for the a- and b-waves. White light pulses of 0.009, 3.0, and 65.0 cd•sm^{-2} were obtained from the light-emitting diodes embedded in the contact lens electrode. The stimulus duration was 0.03, 3.0, and 5.0 ms for 0.009, 3.0, and 65.0 cd•sm^{-2}, respectively. The interstimulus interval was 2 seconds for 0.009 cd•sm^{-2} and 15 seconds for the two higher intensities.

To isolate the cone pathway, mice were exposed to a white adapting field of 25 cd•m^{-2} for 10 minutes, and the photopic and flicker ERGs were elicited by white light pulses of 3 ms delivered at a frequency of 1 and 10 Hz. The stimuli were presented on the white adapting field. Five to fifteen responses were averaged for the single-flash ERGs, and 15 responses for the 10-Hz flicker ERGs. The amplitude of the a-wave was measured from baseline to the trough of the a-wave, and the b-wave was measured from the trough of the a-wave to the peak of the b-wave. The implicit time was measured from the onset of the stimulus to the peak of the a- or b-waves.

Retinal Morphometry and Electron Microscopy

The enucleated eyes were immediately embedded in optimal cutting temperature (OCT) compound (Lab-Tek Products, Naperville, IL) and frozen in dry ice-ethanol for cryosectioning. The sections were stained with hematoxylin and eosin. Horizontal sections were cut through the optic nerve, and sections were obtained from WT and *Sod1*$^{-/-}$ mice (KO) at 10, 30, and 50 weeks of age (n = 10, each group). Sections with at least 20 rows of inner nuclear cell layer (INL) and outer nuclear cell layer (ONL) were selected, and the number of nuclei/column was calculated as described with slight modifications.[15] The ratios of the number of nuclei in the *Sod1*$^{-/-}$ to WT (*Sod1*$^{-/-}$/WT) numbers were used for the statistical analyses. For transmission electron microscopy, tissues were fixed, prepared, and observed as previously reported.[11]

Terminal Deoxynucleotidyl Transferase-Mediated dUTP Nick End Labeling (TUNEL) Staining

TUNEL was performed to detect apoptosis in the retina with the *in situ* cell death detection kit, POD (Roche Molecular Biochemicals, Indianapolis, IN). Briefly, frozen sections were fixed in 4% paraformaldehyde in phosphate-buffered saline (PBS) and incubated in 0.1% Triton X-100 and 0.1% sodium citrate for 2 minutes at 4°C, rinsed twice in PBS, followed by incubation in 0.3% H_2O_2-containing methanol for 30 minutes at room temperature to block the endogenous POD activity. After washing in PBS, sections were incubated with the TUNEL reaction mixture containing terminal deoxynucleotidyl transferase in a moist chamber overnight at 4°C, washed again with PBS, and incubated with TUNEL POD for 1 hour at room temperature. To make the apoptotic cells visible, sections were incubated with 3′-diaminobenzidine as a chromogen and counter stained with hematoxylin.

Western Blots and Immunohistochemistry for Caspase

Western blot analysis for procaspase-3 and cleaved caspase-3 was performed with retina lysates. Briefly, retinas were sonicated in 0.5% Nonidet P-40, 10 mmol/L Tris-HCl (pH 7.5), and 150 mmol/L NaCl containing Complete Protease Inhibitor cocktail (Roche Diagnostics GmbH, Mannheim, Germany). Tissue homogenates were centrifuged at 15,000 × g for 30 minutes, and equal amounts (20 μg) of tissue extract were added to 15% sodium dodecyl sulfate-polyacrylamide gel electrophoresis and electroblotted onto an Immobilon-P membrane (Millipore, Bedford, MA). The membranes were blocked in 5% skim milk in Tris-buffered saline and probed with antibodies against caspase-3 (1 1000, 8G10; Cell Signaling, Danvers, MA). Immunoreactive procaspase-3 and cleaved caspase-3 were made visible with the ECL system (Amersham Biosciences, Piscataway, NJ) and luminoimage analyzer LAS-3000 (Fuji Film, Tokyo, Japan). For control, confluent NIH 3T3 cells were treated and incubated with 1 μmol/L staurosporine for 8 hours, and cell lysates were analyzed. Immunohistochemistry with anti-cleaved caspase-3 antibody (no. 9661, Cell Signaling) were performed for WT and KO with different ages (10 weeks, 30 weeks, and 50 weeks), following the manufacturer's protocol. Nuclei were counterstained with 4,6-diamidino-2-phenylindole. Sections were prepared from mammary tissues from 2-week-old mice after weaning to obtain positive controls.

Statistical Analyses

Data are presented as the means ± SE of the means (SEMs), and analyzed with Student's t-tests. For the thick-

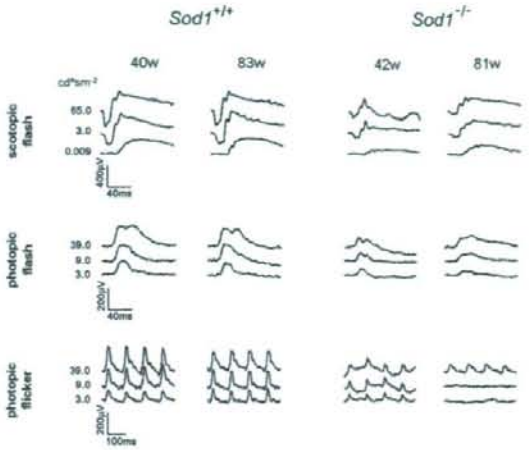

Figure 1. ERGs recorded from age-matched WT and *Sod1*$^{-/-}$ mice. Data of two representative cases of the WT and two *Sod1*$^{-/-}$ mice are shown. ERGs were recorded under three different stimulus conditions (scotopic flash, photopic flash, photopic flicker). Stimulus intensities are shown at the **left**.

ness of the ONL and INL. Kruskal-Wallis test followed by Bonferroni post hoc test was performed to evaluate differences at all periods. A P value <0.05 was considered statistically significant.

Results

ERGs

Representative scotopic, photopic, and 10-Hz flicker ERGs recorded from a 42-week-old mouse and an 81-week-old *Sod1*$^{-/-}$ mouse, and a 40-week-old mouse and an 83-week-old WT mouse are shown Figure 1. The ERGs were elicited by different stimulus intensities. At present, it is known that the scotopic a-wave originates from the activity of rods, and the scotopic and photopic b-waves from a depolarization of the on-bipolar cells and potassium efflux from the Mueller cells. The photopic ERGs and the 10-Hz flicker responses originate from the cones and cone-driven bipolar cells.

Our recordings showed that both the a- and b-waves were reduced at the age of 40 weeks. The reduction in the a- and b-waves in *Sod1*$^{-/-}$ mice was found at all stimulus intensities (Figure 2). The ages of the mice in each group were as follows [mean ± SE (range)]: 59.1 ± 7.6 (39.9 to 82.6) weeks in WT, and 57.9 ± 6.4 (42.4 to 80. 5) weeks in KO. At younger ages, ie, <20 weeks, the amplitudes of the ERGs in the two groups were not significantly different. However, the amplitudes of the scotopic a-waves (Figure 3A) and b-waves (Figure 3B) gradually decreased with increasing age in the *Sod1*$^{-/-}$ mice. Therefore, senescent *Sod1*$^{-/-}$ mice exhibited functional disturbances of both the outer and inner sensory retina. It is interesting that the oscillatory potentials were preserved even in a very old *Sod1*$^{-/-}$ mouse showing decreased amplitudes of a- and b-waves (Figure 1).

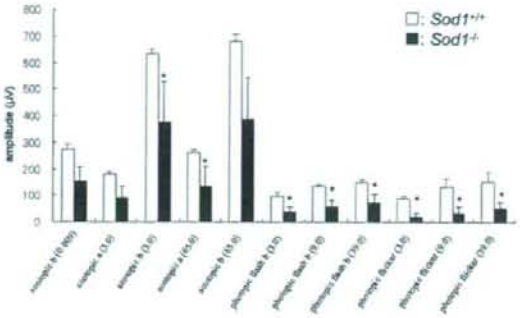

Figure 2. Mean amplitudes of a- and b-waves of the ERGs. ERGs were recorded from age-matched WT and *Sod1*$^{-/-}$ mice ≥40 weeks of age (n = 5, each group). **Asterisk** indicates $P < 0.05$. **White box**, WT; **black box**, *Sod1*$^{-/-}$.

Retinal Histology and Ultrastructure

The thicknesses of the retinal layers of WT and the *Sod1*$^{-/-}$ mice at 10, 30, and 50 weeks of age were measured. The differences in the thicknesses of the INL and ONL were not significant for the two types of mice up to the age of ~10 weeks. Thereafter, the thickness of the ONL and INL in *Sod1*$^{-/-}$ mice gradually decreased (Figure 4). The ratios (KO/WT) of the numbers of nuclei per row were 100.4%, 97.9%, and 81.4% in the INL, and 93.6%, 85.2%, and 71.9% in the ONL at ages 10, 30, and 50 weeks, respectively. The significant decrease in the thickness started at 50 weeks in the INL ($P < 0.01$) and 30 weeks in the ONL ($P < 0.05$), indicating that the photoreceptors, horizontal, bipolar, amacrine, and Mueller cells were most likely damaged in the senescent *Sod1*$^{-/-}$ mice.

Ultrastructural examination showed a disorganized INL and ONL in 15-month-old senescent *Sod1*$^{-/-}$ mice (Figure 5, A–F). The nuclei were swollen, the cytoplasm was vacuolized, and the plasma and nuclear membranes in the INL were disrupted in a *Sod1*$^{-/-}$ mouse at 15 months of age (Figure 5, A and B). The ONL was also disorganized in contrast to the orderly alignment of each column of nuclei in the WT, and the density also decreased in the *Sod1*$^{-/-}$ mice (Figure 5, C and D). The mitochondria in the ONL were damaged, and the cell bodies were swollen. Necrotic cells were also observed (Figure 5F). We rarely observed retinal cells showing chromatin condensation, a morphological hallmark of apoptotic cell. These findings suggest that the death of the neurons in *Sod1*$^{-/-}$ mice was attributable to necrosis, possibly because of elevated ROS.

Cell Deaths in Retinas of Senescent *Sod1*$^{-/-}$ Mice Is Not Caspase-3-Dependent

To explore the mechanism of cell death, we first examined if the apoptotic pathways were activated in retinas of *Sod1*$^{-/-}$ mice at ages 30 and 50 weeks. TUNEL staining showed that the difference between the WT and *Sod1*$^{-/-}$ mice was not significant (data not shown). Next, we performed Western blot analysis for the detection of the

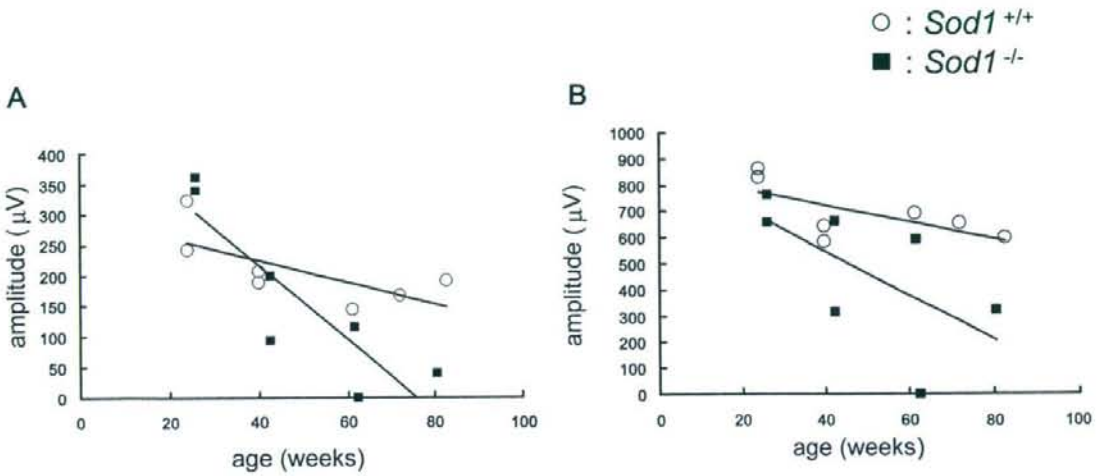

Figure 3. Age-related changes of ERGs. **A:** Age-related changes of the amplitudes of the scotopic a-wave. The amplitudes decrease with increasing age in *Sod1*$^{-/-}$ mice (**black squares**), in contrast to those of the WT (**white circles**). **B:** Age-related changes of the scotopic b-wave. Stimulus intensity was 65.0 cd*sm^{-2}.

active form of caspase, however the activated form of caspase-3 was not apparent in the *Sod1*$^{-/-}$ mice. Immunohistochemistry with anti-cleaved caspase-3 antibody did not show apparent positive signals in the sensory retinas of KO and WT mice as compared with a positive control (data not shown). Therefore, the retinal degeneration of *Sod1*$^{-/-}$ mice appears not to be dependent mainly on apoptosis as in some other models of retinal degeneration.[6–8] Considering that SOD1 is the most abundant antioxidant that scavenges superoxide in retina, cell deaths in ONL of *Sod1*$^{-/-}$ mice might be caused by the ROS-mediated necrotic pathway, rather than by the apoptotic pathways, as was compatible with the ultrastructural findings. Because the presence of inflammatory reactions is a hallmark of necrosis, diffuse deposition of immunoglobulins in retina-retinal pigment epithelium complex in *Sod1*$^{-/-}$ mice[11] might be attributable to necrotic reactions. However, we are aware of the possibility that very slow apoptotic cell deaths could contribute to the retinal dysfunction in these mice.

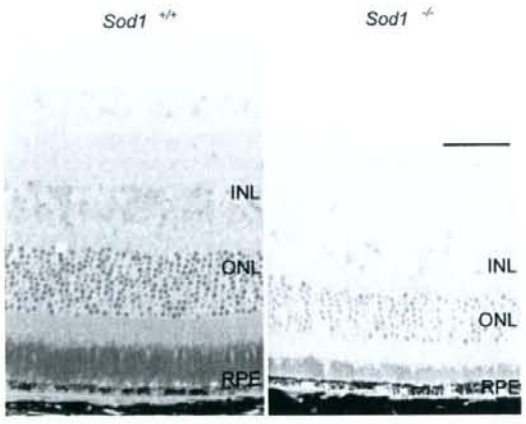

Figure 4. Retinal thinning of *Sod1*$^{-/-}$ mice. Toluidine blue stained retina Quetol 812 sections (2 μm) of a 15 month old WT mouse and an age-matched *Sod1*$^{-/-}$ mouse. Thinning of the INL and ONL is apparent. Scale bar = 50 μm.

Discussion

Our results showed that retina of SOD1-deficient mice had morphological and functional alterations that increased with increasing age. When mice were young (<5 months), the retinas appeared not significantly different from those of WT mice when examined by ophthalmoscopy.[11]

Different Roles of SOD1 and SOD2 in Retina

SOD1 and SOD2 are two major intracellular SODs and both are ubiquitously distributed in the sensory retina.[11] The retinas of *Sod2*$^{-/-}$ mice are thinner than the same age WT mice even at birth.[16] Because *Sod2*$^{-/-}$ mice die soon after birth by dilated cardiomyopathy,[17] *Sod2*$^{-/-}$ mice are not suitable for the examination of age-related retinal dysfunction attributable to accumulated ROS. Current technical modalities for conditional knockout of SOD2 would be expected to overcome this problem.[18] In contrast to the acute and severe retinal degeneration in *Sod2*$^{-/-}$ mice, the degeneration in *Sod1*$^{-/-}$ mice is mild and slowly progressive. Because the amounts of SOD2 and SOD3 proteins are approximately the same in WT and *Sod1*$^{-/-}$ mice,[11] other oxidative stress scavenger systems such as SOD2 may at least partially protect the retina against ROS-mediated retinal damages in *Sod1*$^{-/-}$ mice *in vivo*.

SOD1 Is Necessary to Prevent Age-Related Degeneration of Sensory Retina

In addition to the retinal changes, the *Sod1*$^{-/-}$ mice have a short lifespan,[9] ovarian dysfunction,[19] liver tumors,[9]

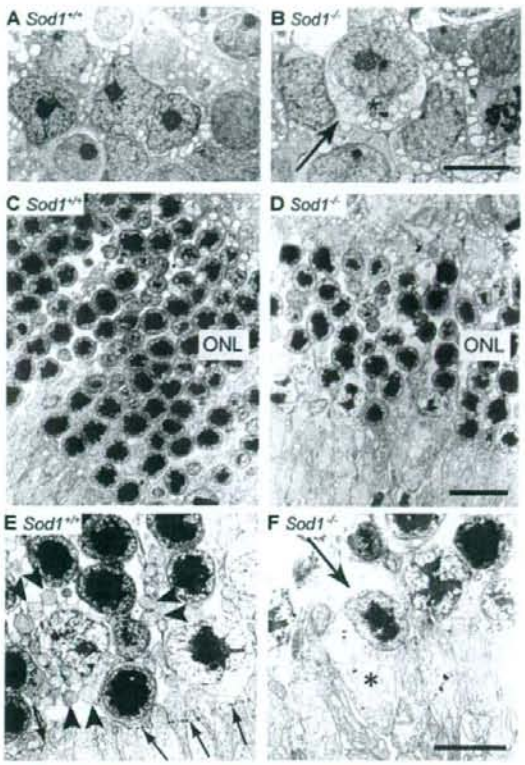

Figure 5. Ultrastructure of sensory retina of the senescent WT and age-matched $Sod1^{-/-}$ mice. **A:** INL of the WT of 15 months. **B:** Swollen nuclei in the INL of age-matched $Sod1^{-/-}$ mice (**asterisk**). Vacuolization and destruction of plasma and nuclear membranes can be seen (**arrow**). **C:** ONL of a WT mouse at 15 months of age. **D:** ONL of an age-matched $Sod1^{-/-}$ mouse. Cell layers are disorganized, and the cell density is decreased. The number of nuclei in the ONL is decreased in $Sod1^{-/-}$ mice. Higher magnification of ONL: WT (**E**), and $Sod1^{-/-}$ mice (**F**). Mitochondria in photoreceptors of ONL distinguished in $Sod1^{-/-}$ mice, as compared with the WT (**arrowheads** in **E**). External limiting membrane in the WT (**arrows** in **E**) is not distinct in a 15-month-old $Sod1^{-/-}$ mouse. Plasma membranes are not clear in a damaged cell of the $Sod1^{-/-}$ mouse (**arrow** in **F**). Swelling of the inner segments of the photoreceptors can be seen (**asterisk**). Scale bars: 2 μm (**B**, **F**); 5 μm (**D**).

anemia,[10] fatty liver,[20] muscle weakness,[21] and hearing loss.[22,23] In addition to the AMD-like phenotypes,[11] we found a novel phenotype of the sensory retina of $Sod1^{-/-}$ mice. The slowly progressive degeneration of the retina appears to resemble the phenotype of the auditory system of $Sod1^{-/-}$ mice. Both the a- and b-waves of the ERGs were reduced in aged $Sod1^{-/-}$ mice. These results are compatible with the retinal histology showing the thinning of the INL and ONL. Because SOD1 is distributed throughout all retinal cell layers,[11] it is not surprising that SOD1 deficiency affected both the INL and ONL.

Recently, a relationship between oxidative stress and retinal degeneration has been reported in animal models. Antioxidants reduce the number of cone deaths in a model of retinitis pigmentosa,[24] and photo-oxidative stress causes retinal degeneration that can be rescued by antioxidants.[25] Our results provide additional evidence that antioxidants may be potentially protective for some types of age-related retinal degeneration. Administration of *N*-acetylcysteine (NAC) can rescue $Sod1^{-/-}$ mice against the effect of anemia by reversing the production of ROS in their erythrocytes.[10] It would be interesting to determine whether the retinal pathologies in $Sod1^{-/-}$ mice can be rescued by antioxidants including NAC, vitamins, or carotenoids. Our results showed no detectable differences in the apoptotic cell death between the retinas of $Sod1^{-/-}$ mice and the WT in the specimens examined. The nuclei of the retinal cells in senescent $Sod1^{-/-}$ mice were swollen suggesting that cell death may be caused by necrosis subsequent to elevated ROS attributable to the absence of SOD1.

Comparison with Other Models of Retinal Degeneration

Many animal models of retinal degeneration have been investigated.[3,4] Apoptosis is observed in some inherited retinal diseases such as retinitis pigmentosa and in other pathological retinal conditions such as hypoxia and oxidative stresses.[26,27] Several genetically mutated models of retinitis pigmentosa have been extensively investigated, including the RCS rat and *rd* mice. The retinal degeneration in the RCS rat is caused by an impairment of retinal pigmented epithelium because of mutation of receptor tyrosine kinase with subsequent photoreceptor cell death. The retinal cell death in RCS rat results from a caspase-1- and -2-dependent apoptosis.[7,27–30] *rd* mice have a recessive mutation of the gene encoding rod cGMP phosphodiesterase β-subunit, and photoreceptor apoptosis also occurs in a caspase-dependent manner.[6] A model of ROS-related retinal degeneration, mice deficient of *uchl3*, has been reported, and they show photoreceptor degeneration with TUNEL-positive cells, which begins at 2 to 3 weeks of age.[8]

These animal models of retinal degeneration differ from $Sod1^{-/-}$ mice; 1) $Sod1^{-/-}$ mice show very slow progressive degeneration, 2) the a- and b-waves are simultaneously affected, and 3) the death of the retinal cells appear to be caused mainly by necrosis rather than apoptosis. Because the $Sod2^{-/-}$ mice are not suitable for long-term follow-up studies,[17] $Sod1^{-/-}$ mice seem to be a good model to study ROS-mediated retinal degeneration. Recently, an intraocular injection of paraquat, a strong pro-oxidant, was reported to induce more severe retinal damage to the retina of $Sod1^{-/-}$ mice than that in the WT. This would indicate that SOD1 may be protective against excessive amounts of exogenous oxidative stress.[31] However, this study did not report the spontaneous retinal changes with age in $Sod1^{-/-}$ mice.

Relevance to Human Retinal Diseases

Oxidative stress is closely associated with retinal degeneration in humans.[32,33] Retinal degeneration is caused by ROS because of iron overload, ie, ocular siderosis.[32] Moreover, AMD is at present considered to be caused by elevated oxidative damages in retina because supple-

mentation by high-dose vitamins and minerals can slow the progression of AMD.[33] Patients with an early stage of AMD have decreased ERGs,[34–39] therefore, *Sod1*$^{-/-}$ mice may mimic the early retinal dysfunction attributable to aging. Excess light to the retina causes retinal degeneration by elevated production of ROS in retina. Therefore, we consider that our findings may help in the understanding of the pathophysiology of the ROS-mediated retinal degeneration in humans. Because nutritional intervention including vitamin A palmitate and ω-3-rich fish slow the progression of disease in many retinitis pigmentosa patients,[40] our findings support the hypothesis that antioxidants may be an additional interventional modality for some types of retinal degeneration.

In summary, we have demonstrated that SOD1 deficiency leads to retinal dysfunction and degenerative changes of retinal cell layers that are progressive. Because senescent *Sod1*$^{-/-}$ mice have choroidal neovascularization, a hallmark of wet-type AMD, *Sod1*$^{-/-}$ mice may exhibit features of both wet- and dry-type AMD. This implies that the etiology of these two clinically distinct entities in humans may be genetically identical.

Acknowledgments

We thank Satoshi Uchiyama, Ichie Kawamori, Yuka Kondo, and Chizuru Tsuda for technical assistance; Eiichiro Nagasaka and Masao Yoshikawa for ERG recording; Junko Moriya and Yumi Takanashi for histology; and Hisao Ohde for helpful discussion.

References

1. Valentine JS, Doucette PA, Potter SZ: Copper-zinc superoxide dismutase and amyotrophic lateral sclerosis. Annu Rev Biochem 2005, 74:563–593
2. Behndig A, Svensson B, Marklund SL, Karlsson K: Superoxide dismutase isoenzymes in the human eye. Invest Ophthalmol Vis Sci 1998, 39:471–475
3. Chang B, Hawes NL, Hurd RE, Davisson MT, Nusinowitz S, Heckenlively JR: Retinal degeneration mutants in the mouse. Vision Res 2002, 42:517–525
4. Dalke C, Graw J: Mouse mutants as models for congenital retinal disorders. Exp Eye Res 2005, 81:503–512
5. Grooten JV, Goossens B, Vanhaesebroeck B, Fiers W: Cell membrane permeabilization and cellular collapse, followed by loss of dehydrogenase activity: early events in tumor necrosis factor-induced cytotoxicity. Cytokine 1993, 5:546–555
6. Hopp RMP, Ransom N, Hilsenbeck SG, Papermaster DS, Windle JJ: Apoptosis in the murine rd1 retinal degeneration is predominantly p53 independent. Mol Vis 1998, 4:5
7. Katai N, Kikuchi T, Shibuki H, Kuroiwa S, Arai J, Kurokawa T, Yoshimura N: Caspase-like proteases activated in apoptotic photoreceptors of Royal College of Surgeons rats. Invest Ophthalmol Vis Sci 1999, 40:1802–1807
8. Sano Y, Furuta A, Seluie R, Kikuchi H, Wang YL, Sakurai M, Kwon J, Noda M, Wada K: Photoreceptor cell apoptosis in the retinal degeneration of Uchl3-deficient mice. Am J Pathol 2006, 169:132–141
9. Elchuri S, Oberley TD, Qi W, Eisenstein RS, Jackson Roberts L, Van Remmen H, Epstein CJ, Huang TT: CuZnSOD deficiency leads to persistent and widespread oxidative damage and hepatocarcinogenesis later in life. Oncogene 2005, 24:367–380
10. Iuchi Y, Okada F, Onuma K, Onoda T, Asano H, Kobayashi M, Fujii J: Elevated oxidative stress in erythrocytes due to a SOD1 deficiency causes anaemia and triggers autoantibody production. Biochem J 2007, 402:219–227
11. Imamura Y, Noda S, Hashizume K, Shinoda K, Yamaguchi M, Uchiyama S, Shimizu T, Mizushima Y, Shirasawa T, Tsubota K: Drusen, choroidal neovascularization, and retinal pigment epithelium dysfunction in SOD1-deficient mice: a model of age-related macular degeneration. Proc Natl Acad Sci USA 2006, 103:11282–11287
12. Goto Y, Peachey NS, Ripps H, Naash MI: Functional abnormalities in transgenic mice expressing a mutant rhodopsin gene. Invest Ophthalmol Vis Sci 1995,36:62–71
13. Sieving PA, Murayama K, Naarendrop F: Push-pull model of primate photopic electroretinogram: a role for hyperpolarizing neurons in shaping the b-wave. Vis Neurosci 1994, 11:519–532
14. Goto Y, Yasuda T, Tobimatsu S, Kato M: 20-Hz flicker stimulus can isolate the cone function in rat retina. Ophthalmic Res 1998, 30:368–373
15. Mori M, Metzger D, Picaud S, Hindelang C, Simonutti M, Sahel J, Chambon P, Mark M: Retinal dystrophy resulting from ablation of RXR alpha in the mouse retinal pigment epithelium. Am J Pathol 2004, 164:701–710
16. Sandbach JM, Coscun PE, Grossniklaus HE, Kokoszka JE, Newman NJ, Wallace DC: Ocular pathology in mitochondrial superoxide dismutase (Sod2)-deficient mice. Invest Ophthalmol Vis Sci 2001, 42:2173–2178
17. Li Y, Huang TT, Carlson EJ, Melov S, Ursell PC, Olson JL, Noble LJ, Yoshimura MP, Berger C, Chan PH, Wallace DC, Epstein CJ: Dilated cardiomyopathy and neonatal lethality in mutant mice lacking manganese superoxide dismutase. Nat Genet 1995, 11:376–381
18. Ikegami T, Suzuki Y, Shimizu T, Isono K, Koseki H, Shirasawa T: Model mice for tissue-specific deletion of the manganese superoxide dismutase (MnSOD) gene. Biochem Biophys Res Commun 2002, 296:729–736
19. Matzuk MM, Dionne L, Guo Q, Kumar TR, Lebovitz RM: Ovarian function in superoxide dismutase 1 and 2 knockout mice. Endocrinology 1998, 139:4008–4011
20. Uchiyama S, Shimizu T, Shirasawa T: CuZn SOD deficiency causes ApoB degradation and induces hepatic lipid accumulation by impaired lipoprotein secretion in mice. J Biol Chem 2006, 281:31713–31719
21. Muller MF, Song W, Liu Y, Chaudhuri A, Pieke-Dahl S, Strong R, Huang TT, Epstein CJ, Roberts LJ II, Csete M, Faulkner JA, Van Remmen H: Absence of CuZn superoxide dismutase leads to elevated oxidative stress and acceleration of age-dependent skeletal muscle atrophy. Free Radic Biol Med 2006, 40:1993–2004
22. MacFadden SL, Ding D, Salvi R: Anatomical, metabolic and genetic aspects of age-related hearing loss in mice. Audiology 2001, 40:313–321
23. MacFadden SL, Ding D, Burkard RF, Jiang H, Reaume AG, Flood DG, Salvi RJ: Cu/Zn deficiency potentiates hearing loss and cochlear pathology in aged 129/CD-1 mice. J Comp Neurol 1999, 413:101–112
24. Komeima K, Rogers BS, Lu L, Campochiaro PA: Antioxidants reduce cone cell death in a model of retinitis pigmentosa. Proc Natl Acad Sci USA 2006, 103:11300–11305
25. Tanito M, Nishiyama A, Tanaka T, Masutani H, Nakamura H, Yodoi J, Ohira A: Change of redox status and modulation by thiol replenishment in retinal photooxidative damage. Invest Ophthalmol Vis Sci 2002, 43:2392–2400
26. Pacione LR, Szego MJ, Ikeda S, Nishina PM, McInnes RR: Progress toward understanding the genetic and biochemical mechanisms of inherited photoreceptor degenerations. Annu Rev Neurosci 2003, 26:657–700
27. Phelan JK, Bok D: A brief review of retinitis pigmentosa and the identified retinitis pigmentosa genes. Mol Vis 2000, 6:116–124
28. D'Cruz PM, Yasumura D, Weir J, Matthes MT, Abderrahim H, LaVail MM, Vollrath D: Mutation of the receptor tyrosine kinase gene Mertk in the retinal dystrophic RCS rat. Hum Mol Genet 2000, 9:645–651
29. Feng W, Yasumura D, Matthes MT, LaVail MM, Vollrath D: Mertk triggers uptake of photoreceptor outer segments during phagocytosis by cultured retinal pigment epithelial cells. J Biol Chem 2002, 277:17016–17022
30. Vollrath D, Feng W, Duncan JL, Yasumura D, D'Cruz PM, Chappelow A, Matthes MT, Kay MA, LaVail MM: Correction of the retinal dystrophy phenotype of the RCS rat by viral gene transfer of Mertk. Proc Natl Acad Sci USA 2001, 98:12584–12589
31. Dong A, Shen J, Krause M, Akiyama H, Hackett AF, Lai H, Campochiaro

PA. Superoxide dismutase 1 protects retinal cell from oxidative damage. J Cell Physiol 2006, 208:516–526
32. Weiss MJ, Hofeldt AJ, Behrens M, Fisher K. Ocular siderosis. Diagnosis and management. Retina 1997, 17:105–108
33. Age-Related Eye Disease Study Research Group. A randomized, placebo-controlled, clinical trial of high-dose supplementation with vitamins C and E and beta carotene for age-related cataract and vision loss: AREDS report no. 9. Arch Ophthalmol 2001, 119:1439–1452
34. Hogg RE, Chakravarthy U. Visual function and dysfunction in early and late age-related maculopathy. Prog Ret Eye Res 2006, 25:249–276
35. Feigl B, Brown B, Lovie-Kitchin J, Swann P. The rod mediated multifocal electroretinogram in aging and in early age-related maculopathy. Curr Eye Res 2006, 31:635–644
36. Gerth C, Delahunt PB, Alam S, Morse LS, Werner JS. Cone-mediated multifocal electroretinogram in age-related macular degeneration progression over a long-term follow-up. Arch Ophthalmol 2006, 124:345–352
37. Jackson GR, McGwin G Jr, Phillips JM, Klein R, Owsley C. Impact of aging and age-related maculopathy on inactivation of the a-wave of the rod-mediated electroretinogram. Vision Res 2006, 46:1422–1431
38. Jackson GR, McGwin G Jr, Phillips JM, Klein R, Owsley C. Impact of aging and age-related maculopathy on inactivation of the a-wave of the rod-mediated electroretinogram. Invest Ophthalmol Vis Sci 2004, 45:3271–3278
39. Chen C, Wu L, Wu D, Huang S, Wen F, Luo G, Long S. The local cone and rod system function in early age-related macular degeneration. Doc Ophthalmol 2004, 109:1–8
40. Hartong DT, Berson EL, Dryja TP. Retinitis pigmentosa. Lancet 2006, 368:1795–1809

Graefes Arch Clin Exp Ophthalmol (2008) 246:949–954
DOI 10.1007/s00417-008-0791-x

RETINAL DISORDERS

Changes in retinal thickness are correlated with alterations of electroretinogram in eyes with central retinal artery occlusion

Kei Shinoda · Kisaburo Yamada · Celso S. Matsumoto · Kenichi Kimoto · Kazuo Nakatsuka

Received: 24 December 2007 / Revised: 7 February 2008 / Accepted: 19 February 2008 / Published online: 19 April 2008

Abstract
Background We investigated the relationship between the retinal thickness and electroretinogram (ERG) components in patients with central retinal artery occlusion (CRAO).
Methods The optical coherence tomographic (OCT) images and ERGs of the nine patients (six men and three women; mean age, 61.8 years) were retrospectively analyzed. The thickness of the inner and outer retinal layers at 1 and 2 mm nasal and temporal to the fovea was measured in the horizontally scanned OCT images. The ratio of the inner layer thickness/sensory retinal thickness (IT/ST ratio) was calculated. The amplitudes of the a- and b-waves of the mixed rod-cone ERGs and the photopic negative response (PhNR) of the photopic ERGs were analyzed. The ratio of the amplitude of each component in the affected eye to that of the healthy fellow eye (a/f ratio) was calculated.
Results In the chronic phase (1 to 8 months after onset, eight eyes), the inner layer was significantly thinner than that in the acute phase (P=0.0147, 0.0076, 0.002, and 0.0003 for 2 mm nasal, 1 mm nasal, 1 mm temporal, and 2 mm temporal respectively, within 5 days of onset, six eyes), while the thickness of outer layer was not significantly changed. The ERGs were recorded 6.4±1.5 days after the onset of CRAO. The median of the a/f ratio was 0.84 in the a-wave, 0.56 in the b-wave, and 0.27 in the PhNR. The IT/ST in the chronic phase was positively correlated with the a/f ratio of the amplitude of the PhNR.
Conclusions Measurement of retinal thickness by OCT can be useful for monitoring the changes following CRAO. The correlation between the retinal thickness, especially inner layer thickness, and the ERG components was determined, suggesting that the PhNR in the acute phase might be a good indicator for predicting the thinning of the damaged retina in the chronic phase.

Keywords Optical coherence tomography · Photopic negative response · Central retinal artery occlusion · Retinal ganglion cell

K. Shinoda · K. Yamada · C. S. Matsumoto · K. Kimoto · K. Nakatsuka
Department of Ophthalmology,
Oita University Faculty of Medicine,
Oita, Japan

K. Shinoda (✉)
Department of Brain and Neuroscience,
Division of Sensory and Locomotive Science, Ophthalmology,
Oita University Faculty of Medicine,
Hasama-machi,
Yufu-shi, Oita 879-5593, Japan
e-mail: shinodak@med.oita-u.ac.jp

Introduction

A central retinal arterial occlusion (CRAO) is one of the most serious vascular obstructive disorders of the eye. A reduction of the b-wave with a preservation of the a-wave of the scotopic electroretinogram (ERG) is well-known to be characteristic of eyes with a CRAO [1–4]. Because a CRAO leads to ischemia of the inner retina, the function of the retinal ganglion cells (RGCs) that are particularly susceptible to retinal ischemia have been studied in eyes after a CRAO [5]. The photopic negative response (PhNR) of the photopic ERGs represents the activity of RGCs and

their axons, and has recently been investigated as a useful indicator of the effect of CRAO on retinal function [6, 7].

Recent improvements in the resolution of the cross-sectional imaging by optical coherence tomography (OCT) has greatly enhanced the ability to detect changes in the morphology of the retina. This increased resolution has provided important information on the morphological changes of the retina in several types of macular diseases including CRAO [8–11]. The ophthalmoscopic changes in the eyes with a CRAO include edema of the retina with a cherry red spot in the acute phase, and by the resolution of the edema and narrowing of retinal vessels, decrease in the depth of the foveal pit, and optic disc atrophy in the chronic phase.

We have retrospectively investigated the changes in the retinal thickness of the macular region obtained by conventional ophthalmoscopy and OCT, and correlated these findings with the changes in retinal function obtained from electroretinographic (ERG) recordings in the acute and chronic phases of CRAO.

Patients and methods

The medical records of eyes diagnosed with a CRAO that were examined at the Oita University Hospital from 2006 to 2007 were analyzed. The procedures used conformed to the tenets of the Declaration of Helsinki, and an informed consent was obtained after an explanation of the procedures from each individual who participated. Eyes with other ocular diseases were excluded.

Optical coherence tomography

OCT had been performed on the posterior fundus in all nine eyes with a unilateral CRAO with a commercially available OCT instrument (3D OCT-1000, Topcon, Tokyo, Japan) by experienced ophthalmologists. In brief, the fundus was scanned with a measuring beam with a 3-dimensional OCT system. This OCT instrument is based on a conventional spectrometer-based Fourier-domain (FD) OCT, and a non-mydriatic fundus camera (TRC-NW200, Topcon, Tokyo, Japan) was integrated into the FD-OCT system to monitor the macular area during the scans. The 3-dimensional data set was acquired using the default setting (512×128) of the raster scan protocol, which scans a 6.0×6.0 mm area of the fundus at a depth of 4.0 mm, rendering horizontal pixel spaces of 11.7 μm and vertical pixel spaces of 46.9 μm.

The measurements of the thickness were done manually using the retinal map mode in the default settings, as shown in Fig. 1. The thickness of the overall sensory retina and the inner retinal layer at 1 and 2 mm nasal and temporal to the fovea in the horizontal cross-sectional images including fovea was measured. The thickness of nerve fiber layer (NFL) was not measured because differentiating the NFL from the RGC layer was difficult in many images, probably due to the edema as shown in Fig. 2. Because the border of the inner nuclear layer and outer plexiform layer (OPL) was difficult to differentiate, the thickness of the inner retinal layer was taken as the distance between internal limiting membrane (ILM) and the outer edge of the OPL (Fig. 1 *middle and right*). The outer retinal layer thickness was calculated by subtracting the thickness of inner retinal layer from the overall thickness of the sensory retina. The ratio of the thickness of the inner retinal layer to the thickness of the sensory retina was arbitrarily named the inner-layer ratio.

Electroretinography

Photopic ERGs were recorded from all eyes after the pupils were fully dilated with topical 0.5% tropicamide and 0.5%

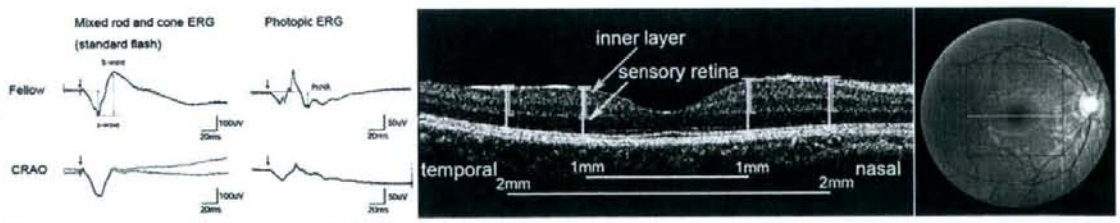

Fig. 1 Representative electroretinograms (ERGs) and optical coherence tomographic (OCT) images. *Left*: ERGs recorded from the normal fellow eye (*upper*) and an eye with a central retinal artery occlusion (CRAO, *lower*). *Middle*: OCT images showing how the retinal layer thicknesses were measured. The thicknesses of the sensory retina and inner retinal layer at 1 and 2 mm nasal and temporal to the fovea in the horizontal cross-section including fovea were measured. Because a clear differentiation of the nerve fiber layer (NFL) and ganglion cell layer (GCL) was difficult in many images, the measurement of the thickness of NFL was not made, and instead the distance between internal limiting membrane (ILM) and the outer edge of the outer plexiform layer (OPL) was measured (indicated by *green arrows*) manually. The thickness of the sensory retina was also measured as the distance between ILM and the high reflective band showing the margin of the inner and outer segments (IS/OS line). PhNR is the photopic negative response. *Right*: Fundus picture showing the scanned area with a *blue square* and crossed line with a *yellow bar*

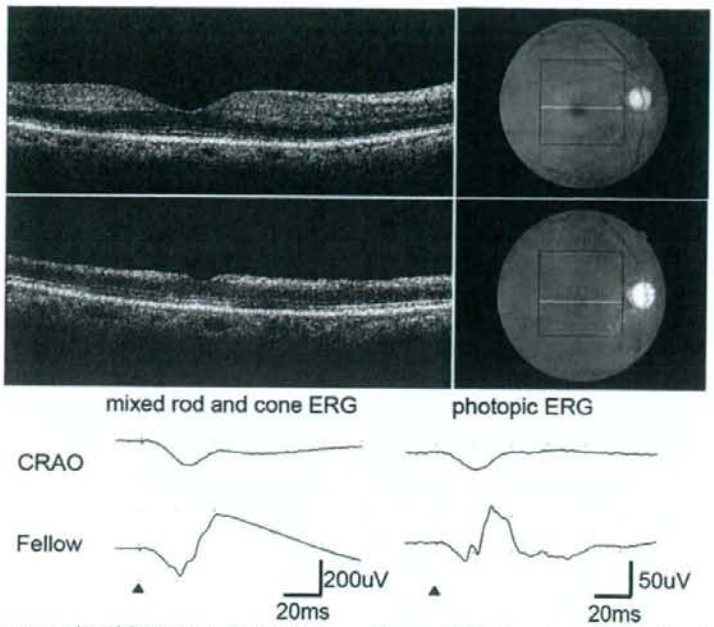

Fig. 2 Optical coherence tomographic (OCT) images, fundus photographs, and electroretinograms (ERGs) from a 74-year-old woman who developed a CRAO in the right eye. The OCT images of the right eye obtained on day 2 (*top*) and 3 months (*middle*) after the CRAO are shown. The corresponding fundus pictures are shown next to each OCT image. In the acute phase (*top*) the fundus shows a cherry red spot and the OCT image shows a thickening of the inner layer. The margin of each retinal layer is difficult to differentiate. In the chronic phase (*middle*), the retina is thinner. The decreased thickness is most obvious in the inner layer, while the outer layer thickness is little affected. The depth of the foveal pit is decreased. The corresponding fundus picture showed optic disc atrophy. The mixed rod-cone ERG and photopic ERG in the affected eye (*upper*) and healthy fellow eye (*lower*) are shown at the bottom. The b-wave of the mixed rod-cone ERG and the photopic negative response (PhNR) of the photopic ERG are non-recordable

phenylephrine hydrochloride. The ERGs were recorded with a corneal bipolar electrode (*Z7285*, Mayo Corp, Japan), and a 10-minute period of light adaptation preceded the photopic ERG recordings. The responses were differentially amplified with a bioamplifier (Neuropack Σ, Nihon Kohden, Japan) with the band pass filters set from 0.1 and 1000 Hz to yield the a- and b-waves and the PhNR. The responses were digitized with a 12-bit A/D board (AD 32/10HD, Contec, Japan), and averaged online, and offline if necessary, using a customized software (Multi Analyser EP, MTS, Japan).

The photopic ERGs were elicited by flashes of white light from high-current type light emitting diodes (LEDs). Bright, short duration (3.0 log cd/m2 with 3 ms duration) white pulses were presented at a frequency of 0.9 Hz on a light-adapting background of 25 cd/m [2]. Four responses were averaged.

Representative photopic ERGs elicited by short and long duration stimuli are shown in Fig. 1 *left*. The amplitudes of the a- and b-waves and the PhNRs, were measured as shown, and the b/a ratio calculated as shown. The ratio of the amplitude in the affected eye to that in the healthy fellow eye, the a/f ratio, was calculated.

Paired *t*-tests were used to determine the significance of the differences in the amplitudes of a- and b-waves and the PhNR between the two eyes. Spearman's correlation of coefficient analysis was performed to determine the correlation between the a/f ratio and the inner layer ratio. A P value <0.05 was considered statistically significant.

Results

There were six men and three women, whose mean age was 61.8 years with a range from 40 to 79 years. At the initial visit, the median duration of the CRAO was 14 hours with a range of 1 hour to 13 days, and the visual acuity ranged from no light perception to 0.04 with a median of hand motion vision. All nine eyes showed re-perfusion on fluorescein angiography (FA). No patients showed choroidal ischemia such as patchy defect or filling delay in choroidal vessels. At the last follow-up examination, the visual acuity ranged from no light perception to 0.2 with a median of counting fingers. Three eyes had a visual acuity ≥0.1. No correlation was found between the visual acuity at the last visit and patients' age.

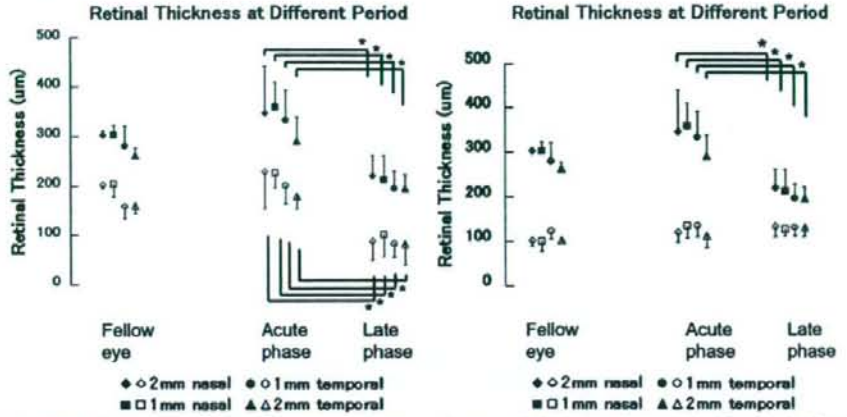

Fig. 3 Changes of retinal layer thickness. The thickness of the sensory retina (*closed symbols*) and inner retinal layer (*open symbols*) appeared to be slightly increased compared to those of healthy fellow eye in the acute phase. The thickness of both layers is significantly thinner in the chronic phase (*left*). The thickness of the outer layer (*open symbols*) is not changed significantly (*right*): $^*P<0.05$. Among the three groups, the Spearman's correlation of coefficient test showed that the amplitudes of the a- and b-waves and the retinal thickness of the inner retina are negatively correlated ($\rho=-0.520$, $P=0.0442$ for a-wave; $\rho=-0.843$, $P=0.0011$, for b-wave)

Six out of the nine patients had hypertension which was well controlled by medication, two had diabetes but without retinopathy, and one had internal carotid artery stenosis. No patients had vasculitis.

The OCT images and photopic ERGs of representative case are shown in Fig. 2.

Optical coherence tomography

OCT images were available from the diseased eye in all nine patients, and from three of the healthy fellow eyes. The OCT images at the acute phase, i.e., within 5 days of onset, were available for six eyes, and at the chronic phase, i.e., 1 to 8 months after onset, for eight eyes. One eye developed a retinal hemorrhage in the macular 2 months after the onset of the CRAO, and the OCT images taken 4 months after onset of CRAO were excluded from the analysis.

The changes in the thickness of the retina are shown in Fig. 3. In the acute phase, when a cherry red spot was still present, the sensory retina and inner retinal layer appeared to be slightly thicker than that of the healthy fellow eye. Unfortunately, the significance of this increase could not be determined because there were data from only three healthy fellow eyes (Fig. 3 *left*). In the chronic phase, the sensory retina and inner layer were significantly thinner that that in the acute phase (the sensory retinal thickness: $P=0.0283$, 0.0257, 0.005, and 0.004 for 2 mm nasal, 1 mm nasal, 1 mm temporal, and 2 mm temporal respectively; the inner layer thickness: $P=0.0147$, 0.0076, 0.002, and 0.0003 for 2 mm nasal, 1 mm nasal, 1 mm temporal, and 2 mm temporal respectively; Fig. 4) The thickness of outer layer did not change significantly (Fig. 3 *right*). No significant correlation between the OCT parameters and visual acuity. No difference was found in the OCT findings concerning the age of the patients.

Electroretinography

ERGs were recorded from the nine eyes with a CRAO and nine of the fellow normal eyes as control. The median interval between the onset of the CRAO and the first ERG

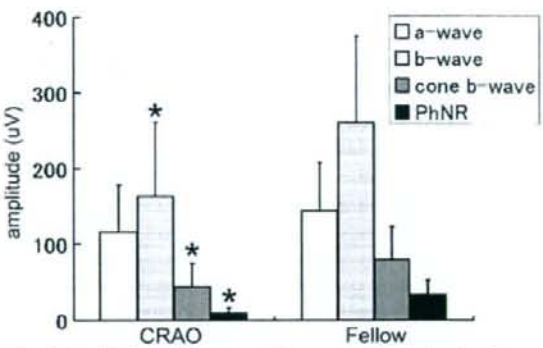

Fig. 4 Amplitudes of the a- and b-waves of the mixed rod-cone electroretinograms (ERGs) and the amplitude of the b-wave and the photopic negative response (PhNR) of the photopic ERG for eyes with a CRAO and for the healthy fellow eye. The amplitudes of the b-wave of the mixed rod and cone ERG in the affected eyes was significantly reduced compared to that in the healthy fellow eye. The amplitude of the a-wave was not significantly different between the eyes. The amplitudes of the b-wave and the PhNR of the photopic ERG in the affected eyes were significantly reduced compared to that in the healthy fellow eye: $^*P<0.05$

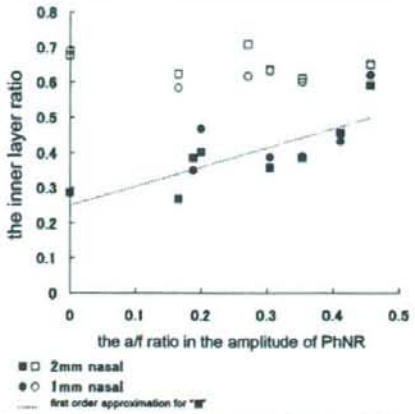

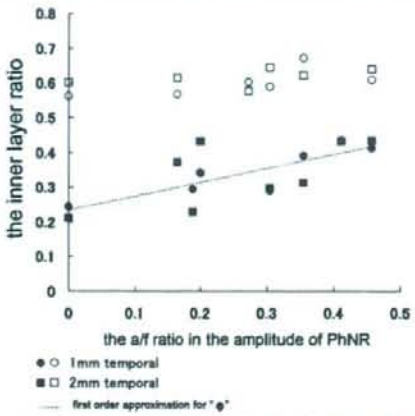

Fig. 5 Plot of the inner layer ratios against the a/f ratios of the photopic negative response (PhNR) amplitude. In the acute phase (*open symbols*), the inner layer ratio was relatively unchanged and independent of the a/f ratio of the PhNR amplitude. However, in the chronic phase (*closed symbols*) the inner layer ratio is correlated significantly and positively with the a/f ratio of the PhNR amplitude at 2 mm nasal from the fovea (P=0.0233, ρ=0.857, Fig. 5 *left*) and at 1 mm temporal from the fovea (P=0358, ρ=0.857, Fig. 5 *right*). The *dotted lines* show the first-order approximation

recordings was 1.5 days. In the mixed rod-cone ERGs, the amplitude of the b-wave in the affected eye was significantly smaller than that of the healthy fellow eye (P=0.0178; paired t-test), whereas the amplitude of the a-wave was not significantly different (P>0.05; paired t-test, Fig. 4). The amplitude of the b-wave of the photopic ERGs was significantly smaller in the affected eye compared to that in healthy fellow eye (P=0.0031; paired t-test, Fig. 4). The amplitude of the PhNR of the photopic ERGs was significantly smaller in the eye with a CRAO than that of the healthy fellow eye (P=0.0014; paired t-test, Fig. 4).

The inner layer ratios are plotted as a function of the a/f ratios of the PhNR amplitude in Fig. 5. In the acute phase, the inner layer ratios were relatively unchanged and not significantly correlated with the a/f ratio of the PhNR amplitude. On the other hand, the inner layer ratio was correlated significantly and positively correlated with the a/f ratio of the PhNR amplitude at the chronic phase 2 mm nasal from the fovea (ρ=0.857, P=0.0233, Fig. 5 *left*) and at 1 mm temporal from fovea (ρ=0.857, P=0.0358, Fig. 5 *right*). The correlation between the inner layer ratio and the a/f ratio of the PhNR amplitude in the chronic phase was not significant at 1 mm nasal from the fovea (ρ=0.786, P=0.0543) and 2 mm temporal from fovea (ρ=0.738, P=0.0508). But no significant correlation was found between the a/f ratio of the PhNR and the visual acuity at the latest visit (P=0.116, Spearman's correlation of coefficient test). No significant correlation was found between the a/f ratio of the b-wave amplitude of the photopic ERG and inner layer ratio in the acute and chronic phases.

For the mixed rod and cone ERG, the correlations between the a/f ratio of the a-wave amplitude and inner layer ratio at the acute and chronic phases were not significant. The correlations between the a/f ratio of the b-wave amplitude and inner layer ratio in the acute and chronic phases were also not significant.

Concerning the difference in the ERG parameters with age, no significant correlation was found between the a/f ratio of the amplitude of a-wave or b-wave (Fig. 6). However, the a/f ratio of the PhNR amplitude had weak but significantly negative correlation with age (p=0.0301, ρ=-0.767, Spearman's correlation of coefficient test). The a/f ratio of the PhNR amplitude was greater in the younger patients (Fig. 6).

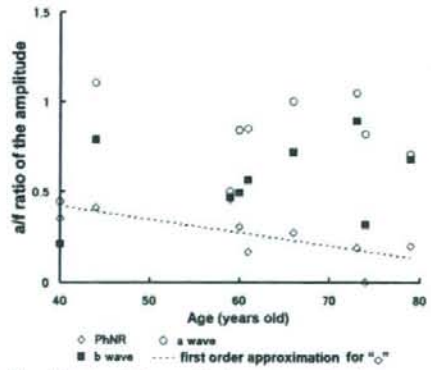

Fig. 6 The a/f ratios of the amplitude against patients' age are plotted. No significant correlation was found between the a/f ratio of the amplitude of a-wave or b-wave and patients' age, whereas the a/f ratio of the PhNR amplitude had negative correlation with age (p=0.0301, ρ=-0.767, Spearman's correlation of coefficient test). The a/f ratio of the PhNR amplitude was greater in the younger patients